

# Multi-Person Respiration Detection: A Digital Programmable Metasurface Analysis Approach

Qun Yan Zhou, Yimiao Sun, Jitong Ma, Yulong Chen, Zi Jun Wang, Si Ran Wang, Jun Yan Dai, Hui-Dong Li,  
Yuan He,*Senior Member, IEEE*, and Qiang Cheng,*Senior Member, IEEE*

**Abstract**—The rapid development of wireless sensing technology has opened new possibilities for non-contact health monitoring. Among them, respiration is crucial information for assessing vital signs. However, traditional methods face challenges of signal interference and overlap in multi-person environments. In this work, we propose a novel method for multi-person respiration detection using a digital programmable metasurface (DPM). This method takes advantage of the modulation characteristics of the DPM in the time and space domain. It divides the Channel State Information (CSI) from the Wi-Fi transmitter into multiple sub-signals in the time domain and modulates the radiation directions of the sub-signals for space redistribution. These signals are received by the Wi-Fi receiver and recombined to restore the CSI in each direction, thus enabling the accurate extraction of respiration signals from targets in different directions. Experimental results show that this method can directionally sense the human respiration information in a specific direction under the static working mode. Under dynamic scanning mode, it can effectively separate and detect the respiration information of four people from different directions. This system has great potential for applications in wireless communication, healthcare, and smart home environments.

**Index Terms**—Digital programmable metasurface, respiration detection, Wi-Fi sensing

Qun Yan Zhou and Yimiao Sun contributed equally to this work. This work was supported by the National Science Foundation (NSFC) for Distinguished Young Scholars of China under Grant 62225108 and 62425207, the National Key Research and Development Program of China under Grant 2023YFB3811502, National Natural Science Foundation of China under Grant U21B2007, the National Natural Science Foundation of China under Grant 62288101, 62201139, and U22A2001, the Fundamental Research Funds for the Central Universities under Grant 2242022k60003, 2242024RCB0005, and 2242024K30009, the Jiangsu Province Frontier Leading Technology Basic Research Project under Grant BK20212002, the Jiangsu Provincial Scientific Research Center of Applied Mathematics under Grant BK20233002, and the 111 Project under Grant 111-2-05, SEU Innovation Capability Enhancement Plan for Doctoral Students under Grant CXJH\_SEU 25076.

Qun Yan Zhou, and Zi Jun Wang are with the State Key Laboratory of Millimeter Waves, Southeast University, Nanjing 210096, China (e-mails: qyzhou@seu.edu.cn, 220240990@seu.edu.cn).

Yimiao Sun, Yulong Chen, and Yuan He are with the School of Software, Tsinghua University, Beijing 100084, China (e-mails: sym21@mails.tsinghua.edu.cn, yl-chen22@mails.tsinghua.edu.cn, heyuan@tsinghua.edu.cn).

Jitong Ma is with the School of Information Science and Technology, Dalian Maritime University, Dalian 116000, China (e-mail: majitong@dlnu.edu.cn).

Si Ran Wang is with the State Key Laboratory of Terahertz and Millimeter Waves, City University of Hong Kong, Hong Kong, China; and the State Key Laboratory of Millimeter Waves, Southeast University, Nanjing 210096, China (e-mail: wang18686568096@163.com).

Jun Yan Dai, Hui-Dong Li, Qiang Cheng are with the State Key Laboratory of Millimeter Waves, Southeast University, Nanjing 210096, China; the Institute of Electromagnetic Space, Southeast University, Nanjing 210096, China; and the Frontiers Science Center for Mobile Information Communication and Security, Southeast University, Nanjing 210096, China. (e-mails: junyand@seu.edu.cn; lihuidong8090@163.com; qiangcheng@seu.edu.cn)

## I. INTRODUCTION

WITH the development of 5G, 6G, and the Internet of Things (IoT), wireless sensing technology has rapidly become an important foundation for the future intelligent society [1]–[4]. This technology utilizes existing wireless networks and adopts advanced methods such as Radio-Frequency Identification (RFID) [5]–[7], Ultra-Wideband (UWB) [8]–[10], Wi-Fi sensing [11]–[13], and millimeter-wave radar [14]–[16]. Without directly contacting the targets, it extracts information by capturing and analyzing the reflection and scattering of wireless signals [17]–[20]. By leveraging the propagation characteristics of wireless signals, wireless sensing can detect and monitor the status and activities of objects in the environment without acquiring images or sounds, providing great flexibility and enhancing privacy protection. Wireless sensing technology transcends the limitations of traditional sensing methods, heralding a new era of the intelligent society characterized by cost reduction, increased flexibility, strong privacy protection, and precise sensing capabilities.

Respiration is a fundamental physiological process, and accurately monitoring respiratory patterns is crucial for diagnosing and managing various health conditions. Traditional respiratory detection methods, such as wearable devices and contact-based sensors, often face limitations in terms of comfort and accessibility [21]–[23]. Wireless sensing technology offers an alternative approach [24]–[27]. By detecting the subtle fluctuations in signals caused by chest expansion and contraction during respiration through wireless signals, the respiratory frequency can be estimated from the scattered signals of the body, enabling remote monitoring without physical contact with the observer. UWB, radar, and RFID have been used to achieve non-contact respiratory sensing [28]–[31]. However, these methods usually require specialized sensing devices and are relatively expensive. With the widespread popularity of Wi-Fi, Wi-Fi-based respiratory detection technology has attracted extensive attention [32]–[37]. The detection task can be accomplished by analyzing the Received Signal Strength Indicator (RSSI) or Channel State Information (CSI) in existing Wi-Fi networks. Among them, Fullbreath applies the conjugate multiplication of CSI between two Wi-Fi antennas to eliminate phase offsets and restore accurate respiratory signals [32]. Farsense proposes a method that uses the ratio of two antennas to break through the range limit of Wi-Fi-based respiratory sensing, significantly increasing the range of Wi-Fi respiratory perception [33]. Wi-Cyclops can capture the CSI changes caused by respiratory movements through a single antenna on a commercial Wi-Fi device for human



Fig. 1. Typical application scenarios of multi-person respiration detection based on DPM-aided Wi-Fi. The DPM works with Wi-Fi terminal to separate and detect breathing information from multiple people in the same space using time and space modulation capabilities.

respiratory sensing in indoor environments [34]. However, the above-mentioned methods can only be implemented in the presence of a single target. In a multi-target environment, the respiration signals from different individuals interfere with each other, making it difficult to accurately distinguish and extract the respiration of each target. Moreover, in real life, as a common wireless device, the Wi-Fi terminal is usually placed in complex living areas, and the number of people in its environment is often random.

Considering the multi-person respiratory detection scenario in complex channel conditions, TinySense uses the time-of-arrival of CSI to filter out the effects of multipath and realizes the respiratory detection of two people [35]. Multisense successfully models multi-person respiratory sensing as a blind source separation problem and simultaneously detects the respiratory information of four people [36]. Based on the IEEE 802.11 standard, Xiong et al. extract respiratory patterns from the Channel Impulse Response (CIR) phase, and simulations verify the centimeter-level positioning accuracy and respiratory perception ability of this method in multi-person scenarios [37]. However, the above-mentioned methods often require more complex algorithms or the usage of large-scale antenna arrays to achieve, which limits the promotion of the system in practical applications.

As a revolutionary two-dimensional structure, metasurface has emerged as a cutting-edge electromagnetic (EM) wave manipulation technology. By designing sub-wavelength artificial structures, metasurfaces can precisely control EM wave prop-

erties such as amplitude, phase, and polarization [38]–[43]. Additionally, DPM have overcome the limitations of fixed-function designs in manufacturing [44]–[46]. DPMs utilize digital coding to represent the different EM responses of the meta-atom. By changing the digital coding, flexible and rapid switching between each state can be achieved. This innovation has paved the way for dynamic real-time manipulation of EM waves and direct information processing, giving rise to applications such as reconfigurable beamforming, information entropy control, wireless communication, and imaging [47]–[52].

With the help of metasurface technology, the application scenarios in wireless environments have been significantly expanded, especially in the field of wireless sensing. In the field of respiratory sensing, researchers have accurately captured the respiratory signals of multiple targets by fully exploiting the space-time modulation characteristics of metasurfaces [53], [54]. However, existing methods face several challenges: the optimization algorithms involved are often complex, and the system stability may be compromised in practice. Moreover, the generation of harmonic signals can interfere with regular wireless channels, necessitating a trade-off between sensing performance and communication quality in practical deployments. Current time-space modulation mechanisms rely on single-tone excitation signals, using the resulting harmonics to sense multiple targets from different directions. Yet this approach has critical limitations. First, single-frequency excitation inherently produces harmonic frequencies that pollute

the spectrum and interfere with existing wireless networks, rendering such methods incompatible with current communication platforms. Second, they require complex real-time optimization to scan the spatial domain across multiple harmonic orders, leading to high computational overhead and stringent hardware demands. Additionally, energy dispersion across multiple harmonics results in low energy efficiency. These limitations underscore the need for more spectrum-friendly, computationally lightweight, and energy-efficient solutions to support scalable and practical wireless sensing applications.

To address the above-mentioned issues, this paper presents a multi-person respiration detection method that applies the DPMs' flexible modulation abilities for EM waves in both time and space dimensions. A typical application scenario is shown in Fig.1. This method takes advantage of the space-time modulation characteristics of DPM to divide the CSI from the Wi-Fi transmitter into multiple sub-signals in the time domain and modulate the radiation directions of the sub-signals for spatial re-distribution. Upon interacting with the human targets in the environment, these signals are received by the Wi-Fi receiver and recombined to restore the CSI in each direction. This enables the accurate extraction of respiration signals from targets in different directions. Practical experiments have verified that, under static working mode, this method can detect the respiration information of targets in a specific direction while filtering out interference from other targets. In the dynamic scanning mode, it can concurrently separate and extract the respiration signals of four individuals. The results show that, without modifying the Wi-Fi structure, this method can effectively separate the respiration features of multiple targets.

The main contributions of this paper are summarized as follows:

(1) We propose a CSI space-time slicing and recombination method based on DPM. By leveraging the space-time modulation characteristics of DPM, the CSI from the Wi-Fi transmitter are divided into multiple sub-signals in the time domain and re-distributed in space. Upon interacting with the targets, these signals are received by the Wi-Fi receiver and recombined to restore the CSI in each direction, thereby enabling the precise extraction of respiration signals from targets in different directions.

(2) We design a DPM with 2-bit phase-modulation functionality in the Wi-Fi frequency band. By controlling the reflection coefficients of its column meta-atoms through digital coding, this DPM can manipulate the Wi-Fi signal to perform single-beam scanning within the  $\pm 60^\circ$  interval, significantly enhancing the signal strength in the designated direction and reducing the scattering energy in other directions.

(3) Based on the designed DPM and the standard Wi-Fi transceiver architecture, we construct a multi-target respiration sensing system based on DPM. The system features two operating modes in multi-person scenarios: static operating mode and dynamic scanning mode. Experiments have verified that the DPM-aided Wi-Fi sensing system can directionally enhance the respiratory signals in the target direction while reducing interference from other directions, thus enabling the effective extraction of multi-person respiratory signals.

The structure of this paper is as follows: In Section 2, we briefly analyze the limitations of existing Wi-Fi-based respiration sensing technologies, focus on discussing the interference problems in multi-person scenarios under the multipath model, and introduce DPM to enhance the scattering energy of specific targets. In Section 3, based on the space-time modulation characteristics of DPM, a CSI space-time slicing and recombination method based on DPM is proposed. A prototype of a DPM-aided Wi-Fi sensing system is then presented, accompanied by the design of a 2-bit DPM tailored to operate within the Wi-Fi frequency band for this system. In Section 4, the comprehensive performance of DPM is validated within an anechoic chamber. Utilizing the designed DPM and the standard Wi-Fi transceiver architecture, the prototype system is constructed and tested in a real-world scenario. The experimental results are meticulously analyzed thereafter. Finally, Section 5 offers a comprehensive summary of the work presented in this paper.

## II. ANALYSIS OF THE LIMITATIONS OF WI-FI RESPIRATION DETECTION

In recent years, Wi-Fi signals have been widely used to monitor health conditions such as human respiration. Among them, Wi-Fi CSI reflects various changes that the Wi-Fi signal experiences during propagation, such as amplitude attenuation, phase shift, and time delay. Under ideal conditions, the CSI signal  $H(f)$  with a central frequency of  $f$  can be given as

$$H(f) = Ae^{-j2\pi \frac{d}{\lambda}}, \quad (1)$$

where  $A$  is the complex attenuation,  $d$  is the length of the propagation path, and  $\lambda$  is the wave length. Fig. 2 (a) shows the schematic diagram of Wi-Fi-based respiration detection. The rhythmic expansion and contraction of the chest during respiration lead to changes in the amplitude and phase characteristics of CSI. By extracting the CSI and using the Variational Mode Decomposition (VMD) algorithm, the respiration signal can be recovered from the Wi-Fi channel information. The Lagrange function  $L(\{u_k\}, \{\omega_k\}, \lambda)$  constructed by the VMD algorithm can be expressed as

$$\begin{aligned} L(\{u_k\}, \{\omega_k\}, \lambda) = & \alpha \sum_{k=1}^K \left\| \partial_t \left[ \left( \delta(t) + \frac{j}{\pi t} \right) * u_k(t) \right] e^{-j\omega_k t} \right\|_2^2 \\ & + \left\| h(t) - \sum_{k=1}^K u_k(t) \right\|_2^2 + \langle \lambda(t), h(t) - \sum_{k=1}^K u_k(t) \rangle, \end{aligned} \quad (2)$$

where  $u_k$  is the  $k$ -th modal component, which is the signal component obtained by decomposition;  $\omega_k$  is the center frequency corresponding to the  $k$ -th modal component;  $h(t)$  is the original time-domain CSI as the signal to be decomposed;  $\lambda(t)$  is the Lagrange multiplier;  $h(t) - \sum u_k(t) = 0$  represents the penalty for the constraint;  $\alpha$  is the smoothing parameter, controlling the smoothness of the decomposed modes;  $\partial_t$  represents the derivative to time  $t$ , calculating the frequency characteristics of the signal;  $\delta(t) + \frac{j}{\pi t}$  is the Hilbert transform kernel, used to obtain the analytic form of the signal;  $\|\cdot\|_2^2$  is the square of the norm. The objective of this Lagrange function

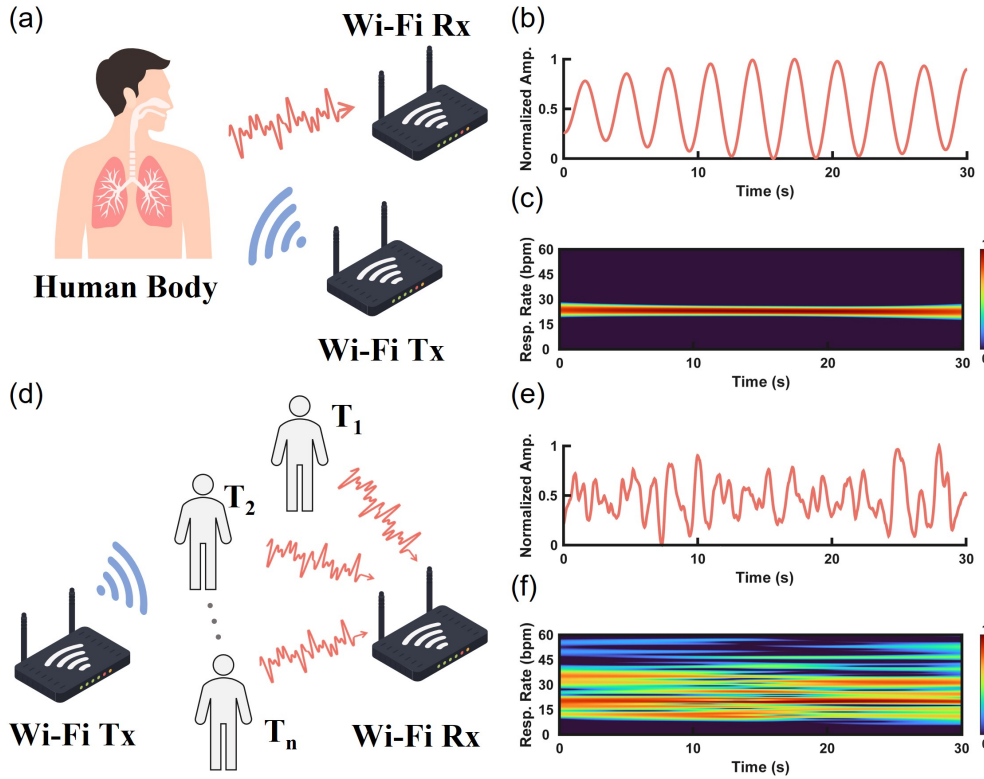


Fig. 2. (a) Schematic diagram of Wi-Fi single-person respiration detection. (b) Time-domain signal of an individual's respiration extracted from Wi-Fi CSI. (c) Spectrogram of an individual's respiration extracted from Wi-Fi CSI. (d) Schematic diagram of Wi-Fi multi-person respiration detection. (e) Time-domain signal of multi-person respiration extracted from Wi-Fi CSI. (f) Spectrogram of multi-person respiration extracted from Wi-Fi CSI.

is to decompose the CSI data received by Wi-Fi into  $k$ -modal components  $u_k$  and ensure that the sum of the decomposed modes is as close as possible to the original signal. After the CSI is processed by the VMD algorithm, the time-domain signal of normal human respiration is shown in Fig. 2(b). It depicts the stability of the respiration rate in the time domain. However, the above-mentioned respiration detection scenario is under ideal conditions. In practical applications, due to the multipath effect, each path will experience different degrees of amplitude attenuation, phase shift, and time delay, resulting in signal overlap at the receiver. In addition, when there are multiple people in the environment, the respiration signals from different people will interfere and overlap, and the finally received CSI can be expressed as

$$H(f) = \sum_{q=1}^Q A_q e^{-j2\pi \frac{d_q}{\lambda}}. \quad (3)$$

In the formula,  $Q$  is the total number of propagation paths, and  $A_q$  and  $d_q$  are the complex attenuation and path length under the  $q$ -th path, respectively. When there are multiple people, the signal emitted by the Wi-Fi Tx will be reflected by different people and received by the Wi-Fi Rx, as shown in Fig. 2(d). In this case, the respiration time-domain signal recovered from the CSI is shown in Fig. 2(e). Due to the interference and overlap of respiration signals from different individuals, the time-domain waveform becomes chaotic, making it difficult to distinguish the respiration waveforms of individual targets.

Fig. 2(f) shows the respiration spectrum in a multi-person scenario. Generally, the normal respiration frequency of an adult is 12 to 20 breaths per minute (bpm). However, due to the superposition of respiration signals from multiple individuals, it is impossible to distinguish the respiration information of each individual from the same time-frequency diagram. Secondly, the aliasing of respiration signals with different frequencies leads to the generation of combined frequencies, contaminating the time-frequency spectrum. In Fig. 2(f), non-normal respiration frequencies can be observed, and it is impossible to judge and separate the respiration characteristics of different targets.

It can be seen that the Wi-Fi-based, multi-person respiration sensing results in a complex multipath environment that is unreliable. The fundamental reason is that the respiration signals of each individual are reflected by multiple paths, interfere with and superimpose on each other, and then are received by the Wi-Fi receiver. The Wi-Fi signals are uncontrollable. Here, we introduce the DPM to artificially manipulate the reflection paths of EM waves. By dynamically regulating the working states of each meta-atom on the DPM, customized manipulation of electromagnetic signals in time and space can be achieved. We propose a new respiration sensing method based on DPM to solve the problems of multipath interference and superposition in Wi-Fi sensing and realize the simultaneous sensing of multi-person respiration signals.

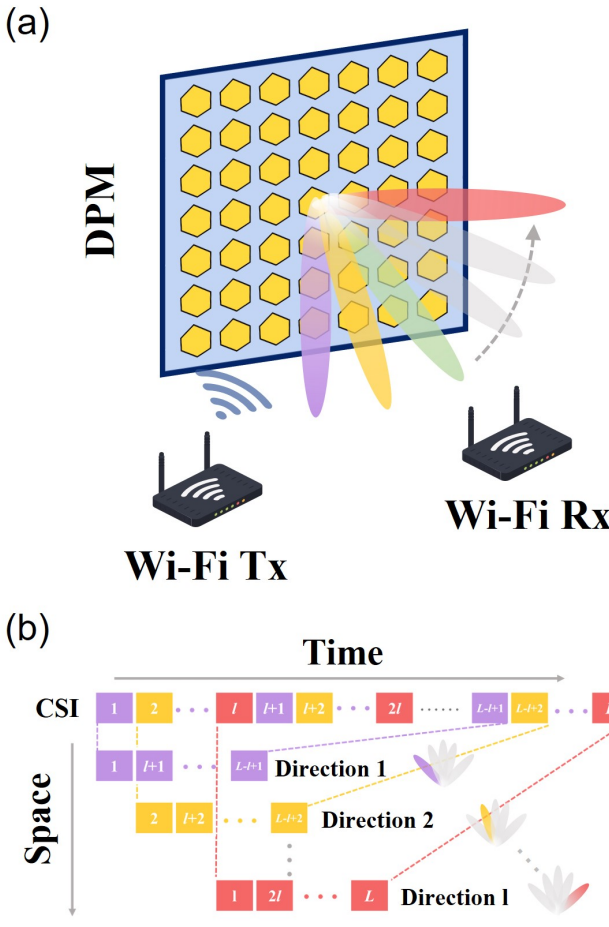


Fig. 3. (a) Schematic diagram of the DPM-aided Wi-Fi system. (b) Schematic diagram of CSI time-space slicing and recombination.

### III. PROPOSED DPM-BASED MULTI-PERSON BREATHING DETECTION METHOD

#### A. DPM-aided Wi-Fi Sensing System Prototype Design

To overcome the interference and mixing of respiration signals from multiple individuals, we propose a cooperative framework between DPM and Wi-Fi terminals to slice and recombine CSI across both temporal and spatial dimensions. Specifically, the DPM is a two-dimensional array composed of reprogrammable meta-atoms embedded with adjustable devices. In the DPM, the reflection phase of the meta-atom can be switched by applying different control voltages. The reflection phase of each meta-atom can be periodically switched according to the corresponding digital binary. For the 1-bit case, the binary representation is "0/1", while for the 2-bit case, it is "00/01/10/11". Here, when a plane wave is incident normally, the far-field function scattered by the DPM can be expressed as:

$$f(\theta, \varphi) = \sum_{m=1}^M \sum_{n=1}^N E_{mn}(\theta, \varphi) \Gamma_{mn} \times e^{-j \frac{2\pi d_{meta}}{\lambda} \sin \theta [(m-1)\cos \varphi + (n-1)\sin \varphi]}, \quad (4)$$

where  $\theta$  and  $\varphi$  are the elevation angle and azimuth angle in an arbitrary direction respectively,  $\Gamma_{mn}$  is the reflection coefficient of the  $(m, n)$ -th meta-atom,  $d_{meta}$  is the spacing between each meta-atom,  $\lambda$  is the wavelength of the central frequency, and  $E_{mn}$  is the meta-atom scattering pattern. By optimizing  $\Gamma_{mn}$  of different meta-atoms, the DPM can achieve different scattering effects, including the directional gain  $G_T$ , which can be expressed as:

$$G_T = \frac{4\pi |f(\theta, \varphi)|^2}{\int_0^{2\pi} \int_0^{\pi/2} |f(\theta, \varphi)|^2 \sin \theta d\theta d\varphi}. \quad (5)$$

By optimizing different  $\Gamma_{mn}$ , the improvement of beam gain in a specific direction can be achieved. Here, we combine the DPM with the Wi-Fi system. We can enhance the energy of a specific-angle path in a multipath environment. In this case, the CSI in Eq. (3) can be modified to

$$H(f) = \sum_{q=1}^{Q-1} A_q e^{-j2\pi \frac{dq}{\lambda}} + G_T A_T e^{-j2\pi \frac{dT}{\lambda}}, \quad (6)$$

where  $A_T$  and  $d_T$  are the complex attenuation and path length along the directional path. This formula shows that after the CSI is redistributed by the DPM, the signal energy in the designated direction is enhanced. When the signal energy is increased to a sufficient extent, Eq. (6) can be further simplified to:

$$H(f) \approx G_T A_T e^{-j2\pi \frac{dT}{\lambda}}. \quad (7)$$

The signal energy after the DPM beamforming is sufficient to overpower the signals from other angles. This enables the enhancement of signal energy in a specific direction and weakens the interference from signals in other directions.

Based on the proposed theory, we put forward a DPM-aided Wi-Fi respiration sensing system. The prototype design of the system is shown in Fig. 3(a). The signal transmitted from the Wi-Fi Tx is spatially redistributed by the DPM. Then it is directed to different directions before being received by the Wi-Fi Rx. The beams in different colors in Fig. 3(a) correspond to different CSI slices, which are redistributed in the designed direction. As indicated by Eq. (7), the extraction of the information of the corresponding CSI slice from the Wi-Fi Rx enables the acquisition of the sensing information in the specific direction and diminishes interference from other directions.

Specifically, we assume that the signal transmitted by the Wi-Fi Tx reaches the DPM. In the time domain, the signal has a total length of  $L$  and is composed of sub-CSI structures each with a length of  $l$ . Here,  $l$  represents the space scanning period of the DPM. Each sub-CSI is further evenly divided into sub-blocks according to space beams and then spatially distributed in various directions by the DPM, which can be expressed as

$$\text{CSI}[n] = \sum_{k=0}^{K-1} \text{CSI}_k[n] \quad n = k \cdot l, k \cdot l + 1, \dots, (k+1) \cdot l - 1 \quad (8)$$

where  $K = L/l$  is the number of sub-CSI blocks. The CSI information in different directions can be further expressed as

$$\text{CSI}_i[n] = \text{CSI}[n] \cdot \text{Beam}_i[n] \quad (9)$$

where  $\text{CSI}_i[n]$  represents the CSI signal of the  $i$ -th direction and  $\text{Beam}_i[n]$  is the beam masking function for the  $i$ -th direction, which can be expressed as

$$\text{Beam}_i[n] = \begin{cases} 1, & \text{if } n \in \text{time slot of direction } i \\ 0, & \text{otherwise} \end{cases} \quad (10)$$

The segmentation result is shown in Fig. 3(b). In the space domain, the CSI received at the receiving end undergoes down-sampling. From the received CSI, the CSI signal in each direction can be separately extracted. Compared with the original CSI, the sampling rate becomes  $1/l$  of the original. Leveraging the space-time modulation capability of the metasurface, the receiver first performs down-sampling on the fully sampled CSI signals. This down-sampling is conducted according to the time cycles allocated by the metasurface in the space domain. Specifically, it extracts CSI signals for each directional target through time-division multiplexing and can be expressed as

$$\text{CSI}_i^{\text{down}}[m] = \text{CSI}_i[m \cdot l] \quad m = 0, 1, \dots, \frac{L}{l} - 1 \quad (11)$$

where  $\text{CSI}_i^{\text{down}}[m]$  represents the downsampled signal for  $i$ -th direction, and the sampling rate is reduced to  $\frac{1}{l}$  of the original rate. The proposed method applies the VMD algorithm to these downsampled CSI signals from different directions, enabling effective extraction of respiratory information.

As long as the Nyquist sampling theorem is satisfied, the respiration signals from each direction can be accurately reconstructed. For example, in Fig. 3(b), the purple CSI block corresponds to a specific spatial direction. During reception, CSI data are downsampled starting from this block at a rate of  $1/l$  relative to the original. These downsampled signals are then recombined to reconstruct the CSI for Direction 1. By processing this reconstructed signal, the system can extract sensing information for that direction. Similarly, this approach can be applied to other directions. Compared with traditional Wi-Fi sensing methods, the proposed DPM-aided approach can sense targets in multiple directions within a single CSI. Moreover, during the sensing process, it can minimize interference from other directions as much as possible, enabling efficient multi-target detection.

### B. The design of the 2-bit DPM

To implement the proposed DPM-aided Wi-Fi sensing system, we designed a DPM with a 2-bit phase quantization operating in the Wi-Fi frequency band. Fig. 4 shows the schematic diagram of the meta-atom of the proposed DPM. The working principle of this DPM is as follows: When irradiated by a far-field source in the upper half-space (where  $z > 0$ ), alterations to the DPM's coding enable the achievement of four distinct coding states. There is a  $90^\circ$  phase difference between adjacent states, while the amplitude remains unchanged.

As shown in Fig. 4(a), the structure of the DPM meta-atom is presented in a 3D view, and its polarization direction

is the x-direction. The meta-atom structure is stacked using printed circuit board (PCB) technology and consists of three layers: the patch layer, the dielectric layer, and the ground layer. The patch layer is composed of an irregular hexagonal patch in the middle and feeder lines on both sides, which are connected through two PIN diodes (MADP-000907-14020x). The dielectric layer is F4B with a thickness of  $H=2.57\text{mm}$  (dielectric constant of 2.65 and loss tangent of 0.02). The ground layer is an unetched metal patch. A metal via in the center of the hexagonal patch penetrates the three-layer structure, connecting the ground planes of the digital and analog signals. The optimal parameter settings of the structure are as follows:  $p=25\text{mm}$ ,  $w_1=12.428\text{mm}$ ,  $w_2=10.235\text{mm}$ ,  $w_3=9.551\text{mm}$ ,  $w_4=15.882\text{mm}$ ,  $w_5=9.297\text{mm}$ ,  $w_6=9.894\text{mm}$ .

Based on the above design, we fabricated a DPM, and the processing result is shown in Fig. 4(c). The entire metasurface contains  $8 \times 8$  meta-atoms, with an overall size of  $150\text{mm} \times 23\text{mm} \times 2.76\text{mm}$ . Two PIN diodes are soldered to each meta-atom. The PIN diodes of each column of meta-atoms share the same bias voltage, and the bias feeder lines on the same side of each column of meta-atoms are connected, sharing the same digital control signal. At the same time, all the ground lines are connected to the metal back-plane of the ground layer. Finally, all the bias feeder lines and ground lines are integrated into a unified interface, which is connected to the control platform via signal lines.

## IV. REAL EXPERIMENT VERIFICATION AND ANALYSIS

To construct the proposed DPM-aided Wi-Fi respiration sensing system, we first tested the EM response of the designed and fabricated 2-bit DPM. By optimizing the digital coding configuration, we evaluated its single-beam scanning performance in space. Subsequently, based on the designed DPM and the standard Wi-Fi system, we built the proposed system. The system we proposed features two working modes: static operating mode and dynamic scanning mode. The static operating mode is used to verify the basic theory and extract the respiratory information of the target in the specified direction at the maximum sampling rate. The dynamic scanning mode reorganizes the CSI time slices and space information, achieving the effect of multi-target detection.

### A. Performance Measurement of the 2-bit DPM

To validate the performance of the designed 2-bit DPM, we tested its EM response and beam-scanning performance in a standard anechoic microwave chamber. The detailed experimental setup is illustrated in Fig. 4(d). A linearly polarized horn antenna operating at 4-8 GHz is placed along the normal direction of the metasurface. They are fixed on a turntable at one end of the anechoic chamber together with the DPM, and they can rotate  $360^\circ$  in the horizontal plane to facilitate the measurement of the scattering pattern. At the other end of the anechoic chamber, a horn antenna with the same linear polarization is fixed to receive the scattering pattern in the horizontal plane.

First, we test the reflection coefficient of the DPM using the free-space method. Horn antenna 1 is connected to a vector

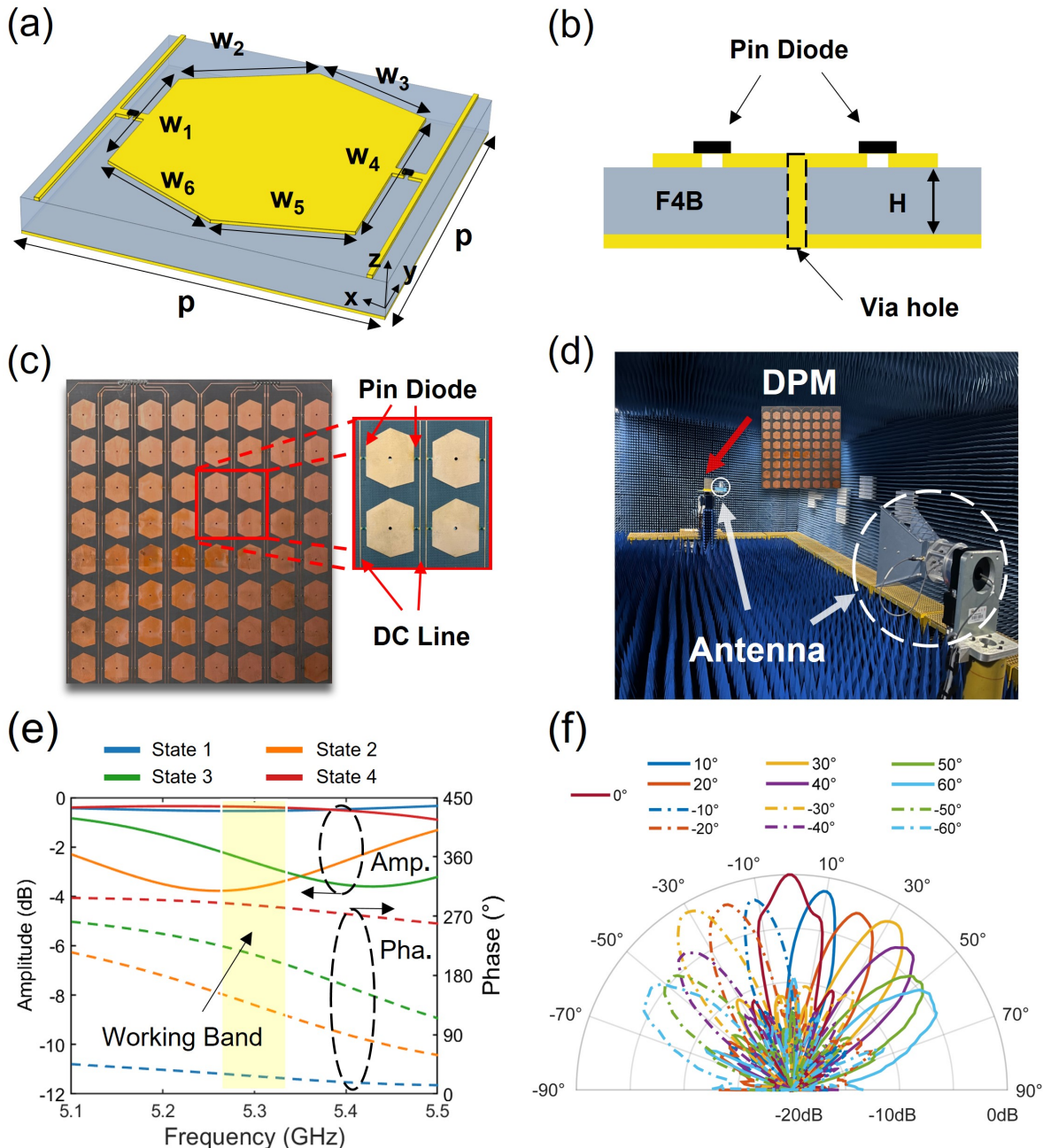


Fig. 4. (a) Meta-atom structure of the DPM. (b) Stacked structure of the DPM meta-atom. (c) Reflection amplitudes and phases of the DPM in four discrete states. (d) The scattering patterns of the DPM with normal incidence in diverse coding states.

network analyzer (Agilent N5245A), and its polarization direction is the same as that of the DPM. By adjusting the digital output voltage through the control platform, we controlled the on/off states of the PIN diodes respectively to test the four states of the DPM. Additionally, depending on the position of the DPM, we set a corresponding time-domain gate in the received signal of the vector network analyzer to filter out the influence of environmental noise on the test results. Fig. 4(d) shows the reflection amplitudes and phases of the DPM in four states within the 5.1-5.5 GHz frequency band. The operating frequency band of this DPM is  $5.3 \text{ GHz} \pm 20 \text{ MHz}$ , and there is a phase difference of  $90^\circ \pm 10^\circ$  between its four states,

meeting the design requirements for operating in the Wi-Fi frequency band. The amplitudes of state 2 and state 3 are relatively low, which may be caused by two factors leading to the non-ideal low reflection amplitudes: 1) Energy dissipation of the F4B substrate due to its high loss tangent of 0.02; 2) In the actual fabricated structure, there is no isolation design between the digital and analog feeding networks, and part of the energy will be coupled into the feeding network.

Subsequently, based on the measured reflection coefficients of the DPM and in combination with the EM scattering model presented in Eq. 4, we optimize the beam coding of the DPM in the range from  $-60^\circ$  to  $60^\circ$  (with an angle interval of  $10^\circ$ )

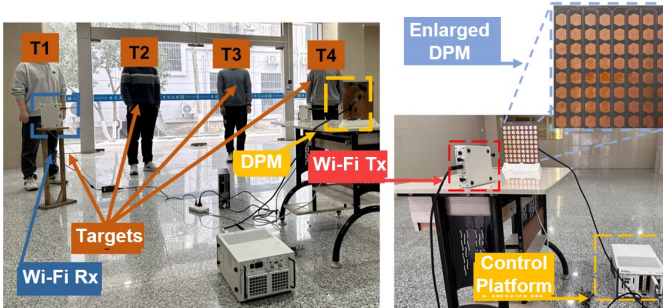


Fig. 5. (a) Experimental scenario for multi-person respiration detection, including four volunteers standing at different angles and the DPM-aided Wi-Fi system. (b) The DPM with DIO lines and a control platform.

using the genetic algorithm. Similarly, we conduct the test in the anechoic microwave chamber. By converting the optimized coding into control voltages, the control platform inputs them to the feeding ports through DIO lines to regulate the coding states of each meta-column. During the test, antenna 1 and antenna 2 are connected to port 1 and port 2 of the vector network analyzer, which is used to provide the feed signal to the DPM and receive the far-field scattering signal, respectively. After performing angle scanning and recording data in the range from  $-60^\circ$  to  $60^\circ$ , the results are shown in Fig. 4(f). The results show that the beam gain of the DPM is around 10 dB in  $-60^\circ$  to  $60^\circ$ . However, as the scanning angle increases, the beam width gradually increases and the gain decreases accordingly. This phenomenon might lead to a reduction of the sensing performance at large angles, with the SNR degrading in comparison to that at small angles. Therefore, this performance change needs to be fully considered in practical applications.

#### B. The Hardware and Software Architecture of DPM-aided Wi-Fi System

We constructed a DPM-aided Wi-Fi transceiver system using the designed 2-bit DPM. This system consists of a pair of Wi-Fi transceivers, the DPM, and its control system. The Wi-Fi transceiver system employs the PicoScenes software-based Wi-Fi signal transceiver platform on USRP, which features easy operation, packet injection, and software-based baseband implementation, meeting the actual testing requirements of Wi-Fi scenarios [55]. PicoScenes is a public platform capable of extracting CSI from 802.11ax frames. This feature is highly consistent with the operational logic of commercial Wi-Fi devices in terms of data processing and signal analysis. As a result, it ensures that the signal interaction and data collection methods in the test environment are identical to those in the actual commercial environment. The DPM is a custom-designed and fabricated one with 2-bit phase modulation capability.

The DPM-aided Wi-Fi system's hardware and software architecture comprises three key components. The 2-bit DPM, which supports discrete phase modulation, is fabricated and connected to a control system via DIO lines. The control system is based on an NI PXIe-1082 chassis, with the NI PXIe-8881 central controller running Labview for task scheduling and data storage, communicating with peripheral modules via

the PXI Express bus. An NI PXIe-6674T timing module manages synchronization, generating sub-microsecond clock signals for precise alignment between the USRP and DPM control system, while the NI PXIe-6581B DIo module outputs 0/1.4V control signals through DIO lines to modulate metasurface. On the FPGA side, LabVIEW FPGA programming on the NI PXIe-7966R maps the metasurface columns to I/O pins, with a hardware timer generating microsecond-precision phase switching sequences and a lookup table converting digital codes to analog voltages for 2-bit phase modulation.

The signal processing workflow is implemented in MATLAB. CSI data collected by the USRP is down sampled to extract direction-specific components, decomposed using the VMD algorithm to isolate respiration-related signals, and then analyzed through short-time Fourier transform to estimate respiratory rates. To achieve precise timing control, the PXIe-6674T timing module exchanges trigger signals with the USRP via external cables. Before each Wi-Fi frame transmission, the USRP sends a GPIO trigger to the timing module, which then generates a precision pulse-per-second (PPS) signal to update the DPM phase profile via the FPGA, ensuring strict synchronization between the Wi-Fi transmission/reception and DPM modulation.

The overall schematic of the entire system is shown in Fig. 5. The Wi-Fi Tx is placed along the normal direction of the DPM, and the Wi-Fi Rx is located at a distant site to collect Wi-Fi signals in space. The antenna polarization directions of the two Wi-Fi terminals are the same as the DPM to ensure efficient modulation of Wi-Fi signals. The CSI packet-sending time is set to 30 s. During the experiment, the volunteers are positioned at different orientations around the metasurface and remain stationary throughout.

#### C. Directional Respiration Detection under Static Operating Mode

The system operates in two modes: static operating mode and dynamic scanning mode. In the static operating mode, the DPM creates a stable phase gradient on its surface to achieve directional beamforming. In a multi-person scenario, it can enhance the respiration signals of the target person in a specific direction while reducing the strength of respiration signals from other directions. In the dynamic scanning mode, the DPM divides the CSI into multiple sub-signals in the time domain. It proceeds to modulate the radiation directions of these sub-signals for scanning multiple people in space. Eventually, at the receiving end, the respiration information of distinct persons in each direction can be sequentially retrieved and reconstructed.

First, we tested the DPM in the static operating mode. In specific scenarios, we prefer to pay attention to the person in a certain direction, minimizing interference from others. The experimental setup remained the same as previously described. In the environment, there were only two individuals. One person stood at an angle of  $30^\circ$  relative to the center of the DPM, while the other stood at  $-20^\circ$ , and both were positioned 3 meters away from the DPM's center. Fig. 6(a) shows the experimental schematic when the DPM is not working. In

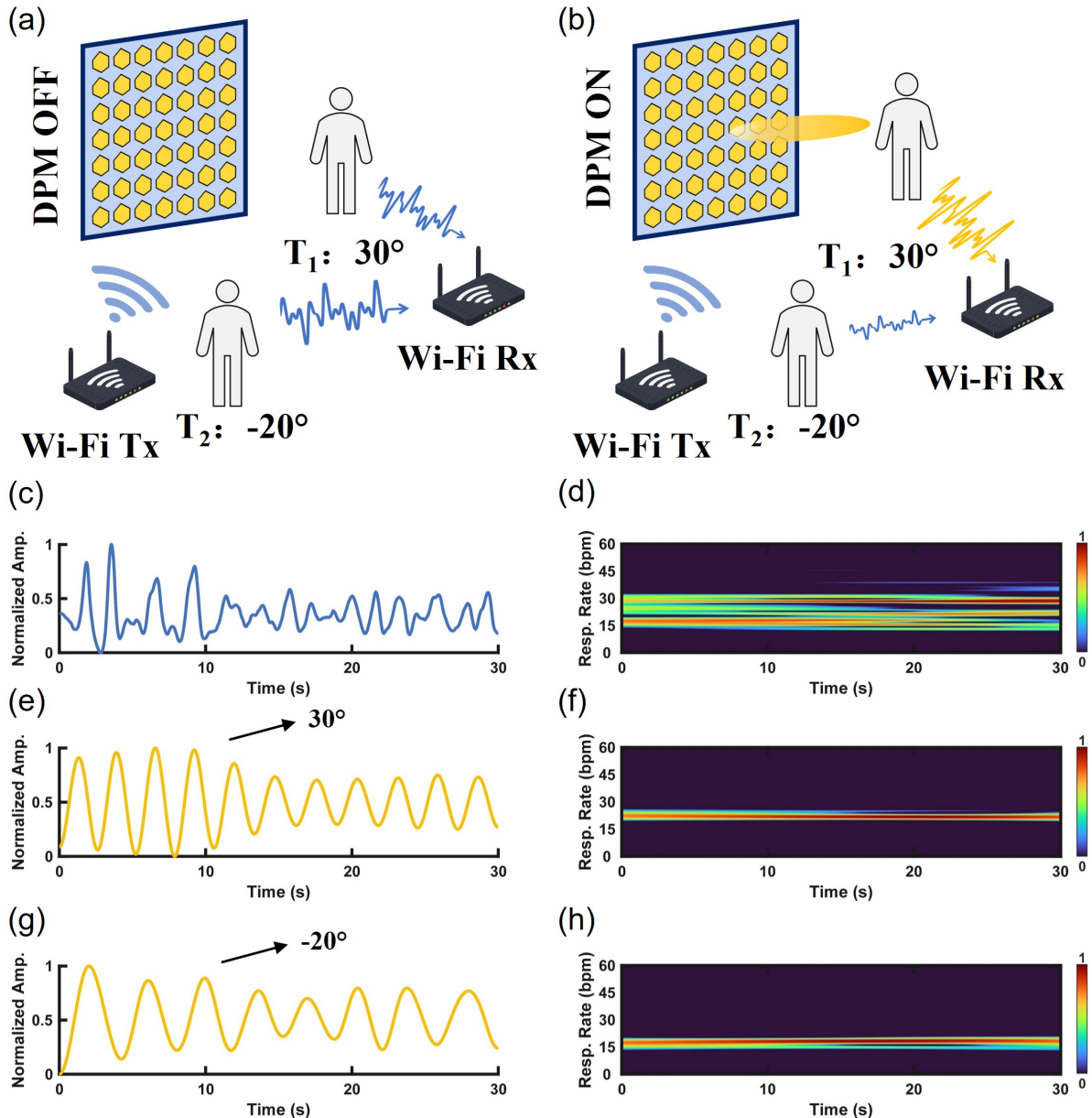


Fig. 6. DPM-aided Wi-Fi respiration detection for two people in a non-operating state. (a) is the experimental schematic diagram, and (c) and (d) are the respiration signal and spectrogram extracted from CIS respectively. DPM-aided Wi-Fi respiration detection for two people in an operating state. (b) is the experimental schematic diagram when the DPM beam is formed to  $30^\circ$ , (e) and (f) are the respiration signal and spectrogram extracted when the target is at  $30^\circ$  respectively, and (g) and (h) are the respiration signal and spectrogram extracted when the target is at  $-20^\circ$  respectively.

this state, all meta-atoms of the DPM have the same coding state, resulting in no beamforming effect. The measured CSI time-domain curve and time-frequency curve are presented in Fig. 6(c) and Fig. 6(d), respectively. These curves exhibit rapid amplitude attenuation, unstable fluctuations, and an ambiguous periodic pattern. At the start, there exist numerous high-frequency components. This indicates the superposition of the respiration signals from multiple targets, rendering the respiration signals impure. Later, the signal amplitude is small, and the fluctuations are irregular, making it difficult to identify the respiration rate. At this time, the time-domain signal waveform has severe aliasing, and it is impossible to effectively extract the respiration signals of each target.

Subsequently, we controlled the DPM to direct the Wi-Fi transmitting beam toward the  $30^\circ$  and  $-20^\circ$  directions, respectively, and recorded the measured CSI time-domain signals and time-frequency curves. The time-domain and time-frequency curves of the target respiration information in the  $30^\circ$  and  $-20^\circ$  directions are shown in Fig. 6(e), (f), Fig. 6(g), and (h), respectively. The respiration rate of target T1 in the  $30^\circ$  direction is detected to be 20 BPM, while that of target T2 in the  $-20^\circ$  direction is 15 BPM. Compared with the mixed respiration signal waveform when the DPM is not working, these two signals have higher amplitude stability and slower attenuation, and are smoother and more regular overall. The waveform has a clear periodicity and less noise, and the

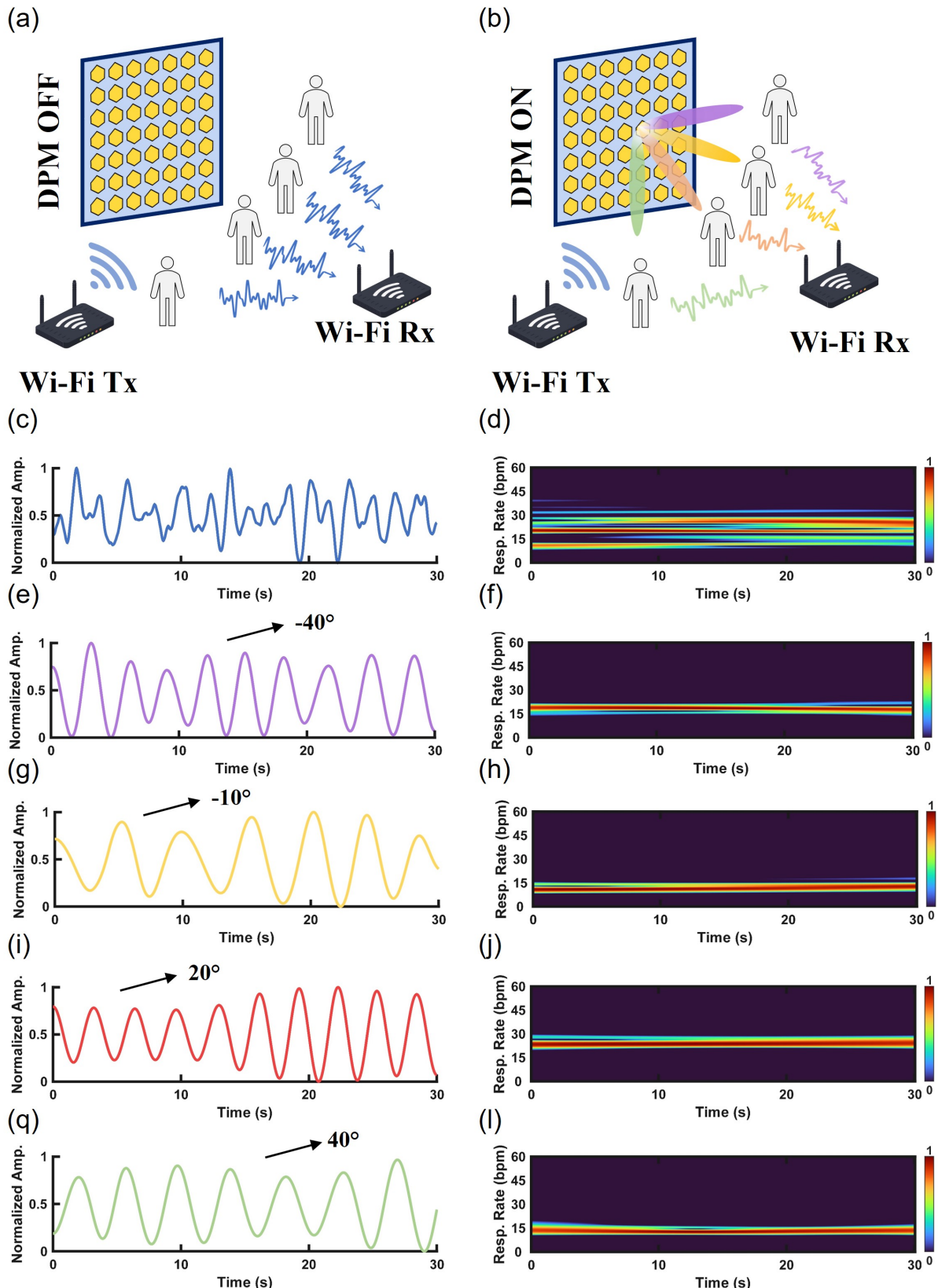


Fig. 7. DPM-aided Wi-Fi respiration detection for four people in Non-working and dynamic scanning mode. (a) and (b) are schematic diagrams of the two states, respectively. (c) and (d) are the respiration signals and the spectrogram in the non-working state, respectively. (e)–(l) are the respiration signals and spectrograms of the four targets extracted at  $-40^\circ$ ,  $-10^\circ$ ,  $20^\circ$ , and  $40^\circ$ .

respiration rate is easier to identify, avoiding the previous phenomena of severe initial fluctuations and later signal weakening. Moreover, these two waveforms maintain good signal quality at different angles, and the measurement stability and anti-interference ability are significantly improved.

The experimental results show that the DPM in the static operating mode can significantly enhance the respiration signals of the target in the specified direction while effectively suppressing the interference from other directions. Compared with the state when the metasurface is not working, the respiration waveform sensed by CSI has a higher amplitude, a more stable periodicity, and significantly improved signal quality. When the metasurface is not used, the signal decays rapidly and has a large amount of noise, making it difficult to extract effective information in the respiration frequency band. This experiment successfully validates the effectiveness of the metasurface technology in enhancing the target respiration signals and suppressing the interference of respiration signals from irrelevant directions.

#### D. Multi-Person Respiration Detection under Dynamic Scanning Mode

The above-mentioned experiments verify that, in the static operating mode, the DPM can achieve directional respiration perception and reduce the respiration interference from other directions. Subsequently, we configured the DPM to the dynamic scanning mode. The experimental environment configuration is shown in Fig. 5(a). Four volunteers are positioned at directions of -40°, -10°, 20°, and 40°, each at a distance of 3 meters from the center of the DPM. According to the optimized DPM space-coding scheme, the DPM controls the Wi-Fi beam to continuously switch in the azimuth from -50° to 50° (a total of 11 sub-beams with an adjacent angle interval of 10°). The CSI packet-sending rate of the Wi-Fi system is 2 ms, and the real-time switching rate of the DPM is 100 Hz. The system can quickly scan different directions and simultaneously capture the respiration information of targets in different directions, improving the real-time performance of perception.

First, we verified the respiration-sensing ability of the original Wi-Fi system in a multi-person scenario when the DPM was in the off state, and Fig. 7(c) and Fig. 7(d) show the CSI time-domain and time-frequency curves. The time-domain signal shows distinct amplitude fluctuations and irregular traits. This reflects the superposition of multiple people's respiration signals, making it arduous to directly extract effective respiratory rhythms. This indicates that it is extremely challenging to completely distinguish the respiration frequencies of various individuals, and a clear-cut separation of targets cannot be achieved. Under the traditional Wi-Fi respiration-sensing method, there are significant signal interference and separation difficulties in CSI respiration sensing in a multi-target scenario.

Subsequently, the DPM operates in the dynamic scanning mode, and the experimental schematic diagram is presented in Fig. 7(b). During the experiment, the DPM divides the CSI of the Wi-Fi transmitter into multiple sub-signals in the

time domain and modulates the radiation directions of the sub-signals for space re-distribution. The Wi-Fi signal is reflected by the DPM and dynamically scanned in space according to the time slices. The signals in a specific direction are enhanced within the corresponding time slices, while the signals in other directions are suppressed. The Wi-Fi Rx receives and extracts the CSI data in different time slices through sampling and then recombines them to restore the human target signals in each angle interval. The respiration time-domain waveforms and time-frequency curves in the -40°, -10°, 20°, and 40° directions perceived by it are shown in Fig. 7(e-l), respectively. In the time-domain diagram, the respiration signal waveforms at different angles show high stability and regularity.

The signal amplitude variations extracted in each direction are smooth, featuring clear periodicity without obvious interference. Compared to when the DPM is off, it can effectively separate respiration signals in multiple directions. The signals' observability and quality improve significantly. In the time-frequency-domain diagram, the respiration signals at each angle are concentrated in the corresponding frequency bands, and the frequency lines are clear and non-overlapping, which indicates that the DPM can effectively suppress other respiration signals from non-target directions, thereby significantly improving the resolution of the signals in the target direction. Compared with the frequency overlap and aliasing problems when the DPM is not used, the DPM successfully achieves accurate discrimination of respiration signals in different directions by our proposed system.

## V. DISCUSSION

In this section, we explore the practical implications of the proposed method's applicability and effectiveness.

### Maximum Supportable Targets Before Performance Degradation:

The corresponding detection beam along this direction has the gain of

$$G(\theta) = N^2 \cdot \text{sinc}^2 \left( \frac{N\pi d}{\lambda} \sin \theta \right) \quad (12)$$

where  $N$  is the column number of the DPM,  $d$  is the column spacing, and  $\lambda$  is the operating wavelength. In our experiment,  $N = 8$ ,  $d = 2.5\text{cm}$ ,  $\lambda \approx 5.3\text{GHz}$ . For sufficient signal separation  $G(\theta_1)/G(\theta_2) \geq 10\text{ dB}$  between the target angle  $\theta_1$  and other angle  $\theta_2$ , the formula shows the angular offset must exceed 15°. Since the proposed system divides the space into 10° intervals, the two targets need to be spaced at least 20° apart. Therefore, the DPM's configuration allows the system to support up to 7 targets simultaneous detections before performance degradation.

**System Performance Under Non-Stationary Conditions:** Although human movement and posture changes may cause signal fluctuations, the metasurface array captures dynamic features in the time-frequency domain. Transient movements or postural adjustments may induce short-term fluctuations in respiratory signals, but when their spectral characteristics do not overlap with the respiratory frequency band, they do not substantially interfere with respiration detection.

**Scalability Analysis:** The angle resolution and beamwidth  $\Delta\theta$  can be expressed as

$$\Delta\theta \approx \frac{0.886\lambda}{Nd \cos \theta} \quad (13)$$

where  $\lambda$  is the wavelength,  $N$  is the column number, and  $d$  is the column spacing. The system's directional support capacity is constrained by the scale of the metasurface array  $8 \times 8$ , where physical limitations of beamwidth and angle resolution in the current configuration define the upper bound of multi-target detection. Scalability positively correlates with the number of array elements  $N$ : increasing the array scale theoretically narrows the beam width. It enhances angle resolution proportionally, allowing for the linear expansion of supportable detection directions and target capacity. However, hardware-level trade-offs exist inherently: higher angular resolution compresses the detection range, while phase distortions induced by target motion in dynamic scenarios significantly degrade detection accuracy.

This study focuses on validating the architecture of DPM-assisted Wi-Fi respiratory detection. Experiments conducted in controlled indoor environments effectively minimize external interference, demonstrating the feasibility of multi-target respiratory monitoring with the proposed hardware setup. Challenges such as multipath interference, Non-Line-of-Sight (NLOS) obstruction, and co-channel signal interference remain common across wireless sensing technologies, presenting clear and promising directions for future exploration within the framework of the proposed architecture.

Future research will explore adaptive multipath cancellation algorithms in conjunction with the spatial modulation capabilities of metasurfaces to enhance system robustness in complex environments. On the hardware side, increasing the number of meta-atoms and optimizing structural designs are expected to improve angular resolution and spatial perception. On the algorithmic side, exploration will include machine learning-based adaptive beamforming and CSI denoising with dynamic target analysis, enabling more accurate extraction of vital signs and real-time tracking of moving individuals.

## VI. CONCLUSION

In this paper, we proposed a Wi-Fi respiration detection approach assisted by DPM. We designed and constructed a respiration detection system based on a 2-bit DPM, which utilizes the time and space modulation capabilities of the DPM to assist the Wi-Fi system, enabling the detection of respiratory signals from multiple people. First, we analyze the problem that spectrum aliasing and interference render existing Wi-Fi-based respiratory sensing methods ineffective when there are multiple targets in the same environment. Subsequently, we leverage the time and space modulation capabilities of the DPM to slice the CSI at different time slots and modulate the radiation directions of the CSI slices for space redistribution. Finally, at the receiving end, the CSI is recombined to restore the CSI sensing signals at different angles. Experiments demonstrate that this method can effectively separate and detect the respiratory signals of four people. In the future, our goal is to conduct further research on multi-person vital

signs sensing with the help of the DPM, especially in scenarios involving moving individuals, such as walking or running. This will further expand its potential applications in various real-world environments.

## REFERENCES

- [1] Fan Liu, Yuanhao Cui, Christos Masouros, Jie Xu, Tony Xiao Han, Yonina C Eldar, and Stefano Buzzi. Integrated sensing and communications: Toward dual-functional wireless networks for 6g and beyond. *IEEE journal on selected areas in communications*, 40(6):1728–1767, 2022.
- [2] Jian Liu, Hongbo Liu, Yingying Chen, Yan Wang, and Chen Wang. Wireless sensing for human activity: A survey. *IEEE Communications Surveys & Tutorials*, 22(3):1629–1645, 2019.
- [3] Jayavaradhana Gubbi, Rajkumar Buyya, Slaven Marusic, and Marimuthu Palaniswami. Internet of things (iot): A vision, architectural elements, and future directions. *Future generation computer systems*, 29(7):1645–1660, 2013.
- [4] John A Stankovic. Research directions for the internet of things. *IEEE internet of things journal*, 1(1):3–9, 2014.
- [5] Roy Want. An introduction to rfid technology. *IEEE pervasive computing*, 5(1):25–33, 2006.
- [6] Roy Want. Enabling ubiquitous sensing with rfid. *Computer*, 37(4):84–86, 2004.
- [7] Filippo Costa, Simone Genovesi, Michele Borgese, Andrea Michel, Francesco Alessio Dicandia, and Giuliano Manara. A review of rfid sensors, the new frontier of internet of things. *Sensors*, 21(9):3138, 2021.
- [8] Jinyun Zhang, Philip V Orlit, Zafer Sahinoglu, Andreas F Molisch, and Patrick Kinney. Uwb systems for wireless sensor networks. *Proceedings of the IEEE*, 97(2):313–331, 2009.
- [9] Ian Oppermann, Lucian Stoica, Alberto Rabbachin, Zack Shelby, and Jussi Haapola. Uwb wireless sensor networks: Uwen-a practical example. *IEEE communications magazine*, 42(12):S27–S32, 2004.
- [10] Qiong Huang, Lele Qu, Bingheng Wu, and Guangyou Fang. Uwb through-wall imaging based on compressive sensing. *IEEE Transactions on Geoscience and Remote Sensing*, 48(3):1408–1415, 2009.
- [11] Jianyang Ding, Yong Wang, Hongyan Si, Shang Gao, and Jiwei Xing. Three-dimensional indoor localization and tracking for mobile target based on wifi sensing. *IEEE Internet of Things Journal*, 9(21):21687–21701, 2022.
- [12] Li Li, Hu Xiaoguang, Chen Ke, and He Ketai. The applications of wifi-based wireless sensor network in internet of things and smart grid. In *2011 6th IEEE Conference on Industrial Electronics and Applications*, pages 789–793. IEEE, 2011.
- [13] Yao Ge, Ahmad Taha, Syed Aziz Shah, Kia Dashtipour, Shuyuan Zhu, Jonathan Cooper, Qammer H Abbasi, and Muhammad Ali Imran. Contactless wifi sensing and monitoring for future healthcare-emerging trends, challenges, and opportunities. *IEEE Reviews in Biomedical Engineering*, 16:171–191, 2022.
- [14] Jürgen Hasch, Eray Topak, Raik Schnabel, Thomas Zwick, Robert Weigel, and Christian Waldschmidt. Millimeter-wave technology for automotive radar sensors in the 77 ghz frequency band. *IEEE transactions on microwave theory and techniques*, 60(3):845–860, 2012.
- [15] Peijun Zhao, Chris Xiaoxuan Lu, Jianan Wang, Changhao Chen, Wei Wang, Niki Trigoni, and Andrew Markham. mid: Tracking and identifying people with millimeter wave radar. In *2019 15th international conference on distributed computing in sensor systems (DCOSS)*, pages 33–40. IEEE, 2019.
- [16] A Soumya, C Krishna Mohan, and Linga Reddy Cenkeramaddi. Recent advances in mmwave-radar-based sensing, its applications, and machine learning techniques: A review. *Sensors*, 23(21):8901, 2023.
- [17] Hugo Landaluce, Laura Arjona, Asier Perallos, Francisco Falcone, Ignacio Angulo, and Florian Muralter. A review of iot sensing applications and challenges using rfid and wireless sensor networks. *Sensors*, 20(9):2495, 2020.
- [18] Paolo Dabone, Vincenzo Di Pietra, Marco Piras, Ansar Abdul Jabbar, and Syed Ali Kazim. Indoor positioning using ultra-wide band (uwb) technologies: Positioning accuracies and sensors' performances. In *2018 IEEE/ION Position, Location and Navigation Symposium (PLANS)*, pages 175–184. IEEE, 2018.
- [19] Yongsen Ma, Gang Zhou, and Shuangquan Wang. Wifi sensing with channel state information: A survey. *ACM Computing Surveys (CSUR)*, 52(3):1–36, 2019.

- [20] J Andrew Zhang, Md Lushanur Rahman, Kai Wu, Xiaojing Huang, Y Jay Guo, Shanzhi Chen, and Jinhong Yuan. Enabling joint communication and radar sensing in mobile networks—a survey. *IEEE Communications Surveys & Tutorials*, 24(1):306–345, 2021.
- [21] Farah Q AL-Khalidi, Reza Saatchi, Derek Burke, Heather Elphick, and Stephen Tan. Respiration rate monitoring methods: A review. *Pediatric pulmonology*, 46(6):523–529, 2011.
- [22] Erik Vanegas, Raul Igual, and Inmaculada Plaza. Sensing systems for respiration monitoring: A technical systematic review. *Sensors*, 20(18):5446, 2020.
- [23] Yunlu Wang, Menghan Hu, Chaohua Yang, Na Li, Jian Zhang, Qingli Li, Guangtao Zhai, Simon X Yang, Xiao-Ping Zhang, and Xiaokang Yang. Respiratory consultant by your side: Affordable and remote intelligent respiratory rate and respiratory pattern monitoring system. *IEEE Internet of Things Journal*, 8(19):14999–15009, 2021.
- [24] Ziheng Mao, Yuan He, Jia Zhang, Yimiao Sun, Yadong Xie, and Xiuzhen Guo. mmhrr: Monitoring heart rate recovery with millimeter wave radar. In *2024 IEEE 30th International Conference on Parallel and Distributed Systems (ICPADS)*, pages 1–8. IEEE, 2024.
- [25] Jia Zhang, Rui Xi, Yuan He, Yimiao Sun, Xiuzhen Guo, Weiguo Wang, Xin Na, Yunhao Liu, Zhenguo Shi, and Tao Gu. A survey of mmwave-based human sensing: Technology, platforms and applications. *IEEE Communications Surveys & Tutorials*, 25(4):2052–2087, 2023.
- [26] Yimiao Sun, Yuan He, Jiacheng Zhang, Xin Na, Yande Chen, Weiguo Wang, and Xiuzhen Guo. Bifrost: Reinventing wifi signals based on dispersion effect for accurate indoor localization. In *Proceedings of the 21st ACM Conference on Embedded Networked Sensor Systems*, pages 376–389, 2023.
- [27] Yulong Chen, Junchen Guo, Yimiao Sun, Haipeng Yao, Yunhao Liu, and Yuan He. Elase: Enabling real-time elastic sensing resource scheduling in 5g vran. In *2024 IEEE/ACM 32nd International Symposium on Quality of Service (IWQoS)*, pages 1–10. IEEE, 2024.
- [28] Yanni Yang, Jianrong Cao, and Yanwen Wang. Robust rfid-based respiration monitoring in dynamic environments. *IEEE Transactions on Mobile Computing*, 22(3):1717–1730, 2021.
- [29] Tauseef Hussain, Sana Ullah, Raúl Fernández-García, and Ignacio Gil. Wearable sensors for respiration monitoring: A review. *Sensors*, 23(17):7518, 2023.
- [30] Hafeez Ur Rehman Siddiqui, Adil Ali Saleem, Imran Bashir, Kainat Zafar, Furqan Rustam, Isabel de la Torre Diez, Sandra Dudley, and Imran Ashraf. Respiration-based copd detection using uwb radar incorporation with machine learning. *Electronics*, 11(18):2875, 2022.
- [31] Shiyu Wu, Siqi Yao, Wei Liu, Kai Tan, Zhenghuan Xia, Shengwei Meng, Jie Chen, Guangyou Fang, and Hejun Yin. Study on a novel uwb linear array human respiration model and detection method. *IEEE Journal of Selected Topics in Applied Earth Observations and Remote Sensing*, 9(1):125–140, 2016.
- [32] Youwei Zeng, Dan Wu, Ruiyang Gao, Tao Gu, and Daqing Zhang. Full-breathe: Full human respiration detection exploiting complementarity of csi phase and amplitude of wifi signals. *Proceedings of the ACM on Interactive, Mobile, Wearable and Ubiquitous Technologies*, 2(3):1–19, 2018.
- [33] Youwei Zeng, Dan Wu, Jie Xiong, Enze Yi, Ruiyang Gao, and Daqing Zhang. Farsense: Pushing the range limit of wifi-based respiration sensing with csi ratio of two antennas. *Proceedings of the ACM on Interactive, Mobile, Wearable and Ubiquitous Technologies*, 3(3):1–26, 2019.
- [34] Youwei Zhang, Feiyu Han, Panlong Yang, Yuanhao Feng, Yubo Yan, and Ran Guan. Wi-cyclops: Room-scale wifi sensing system for respiration detection based on single-antenna. *ACM Transactions on Sensor Networks*, 20(4):1–24, 2024.
- [35] Pei Wang, Bin Guo, Tong Xin, Zhu Wang, and Zhiwen Yu. Tinysense: Multi-user respiration detection using wi-fi csi signals. In *2017 IEEE 19th International Conference on e-Health Networking, Applications and Services (Healthcom)*, pages 1–6. IEEE, 2017.
- [36] Youwei Zeng, Dan Wu, Jie Xiong, Jinyi Liu, Zhaopeng Liu, and Daqing Zhang. Multisense: Enabling multi-person respiration sensing with commodity wifi. *Proceedings of the ACM on Interactive, Mobile, Wearable and Ubiquitous Technologies*, 4(3):1–29, 2020.
- [37] Haoqiu Xiong, Zhuangzhuang Cui, Mingqing Liu, Yang Miao, and Sofie Pollin. Multi-person localization and respiration sensing under ieee 802.11 ay standard. In *Proceedings of the 3rd ACM MobiCom Workshop on Integrated Sensing and Communications Systems*, pages 31–36, 2023.
- [38] John B Pendry, David Schurig, and David R Smith. Controlling electromagnetic fields. *science*, 312(5781):1780–1782, 2006.
- [39] Qiang Cheng, Lei Zhang, Jun Yan Dai, Wankai Tang, Jun Chen Ke, Shuo Liu, Jing Cheng Liang, Shi Jin, and Tie Jun Cui. Reconfigurable intelligent surfaces: Simplified-architecture transmitters—from theory to implementations. *Proceedings of the IEEE*, 110(9):1266–1289, 2022.
- [40] Li-Hua Gao, Qiang Cheng, Jing Yang, Shao-Jie Ma, Jie Zhao, Shuo Liu, Hai-Bing Chen, Qiong He, Wei-Xiang Jiang, Hui-Feng Ma, et al. Broadband diffusion of terahertz waves by multi-bit coding metasurfaces. *Light: Science & Applications*, 4(9):e324–e324, 2015.
- [41] Lixiang Liu, Xueqian Zhang, Mitchell Kenney, Xiaoqiang Su, Ningning Xu, Chunmei Ouyang, Yunlong Shi, Jianguang Han, Weili Zhang, and Shuang Zhang. Broadband metasurfaces with simultaneous control of phase and amplitude. *Advanced materials*, 26(29):5031–5036, 2014.
- [42] Bo O Zhu, Junming Zhao, and Yijun Feng. Active impedance metasurface with full 360 reflection phase tuning. *Scientific reports*, 3(1):3059, 2013.
- [43] Davide Ramaccia, Dimitrios L Sounas, Andrea Alu, Alessandro Toscano, and Filiberto Bilotti. Phase-induced frequency conversion and doppler effect with time-modulated metasurfaces. *IEEE Transactions on Antennas and Propagation*, 68(3):1607–1617, 2019.
- [44] Tie Jun Cui, Mei Qing Qi, Xiang Wan, Jie Zhao, and Qiang Cheng. Coding metamaterials, digital metamaterials and programmable metamaterials. *Light: science & applications*, 3(10):e218–e218, 2014.
- [45] Tie Jun Cui, Shuo Liu, and Lei Zhang. Information metamaterials and metasurfaces. *Journal of materials chemistry C*, 5(15):3644–3668, 2017.
- [46] Shuo Liu and Tie Jun Cui. Concepts, working principles, and applications of coding and programmable metamaterials. *Advanced Optical Materials*, 5(22):1700624, 2017.
- [47] Linlin Li, Hengxin Ruan, Che Liu, Ying Li, Ya Shuang, Andrea Alù, Cheng-Wei Qiu, and Tie Jun Cui. Machine-learning reprogrammable metasurface imager. *Nature communications*, 10(1):1082, 2019.
- [48] Jie Zhao, Xi Yang, Jun Yan Dai, Qiang Cheng, Xiang Li, Ning Hua Qi, Jun Chen Ke, Guo Dong Bai, Shuo Liu, Shi Jin, et al. Programmable time-domain digital-coding metasurface for non-linear harmonic manipulation and new wireless communication systems. *National science review*, 6(2):231–238, 2019.
- [49] Si Ran Wang, Jun Yan Dai, Qun Yan Zhou, Jun Chen Ke, Qiang Cheng, and Tie Jun Cui. Manipulations of multi-frequency waves and signals via multi-partition asynchronous space-time-coding digital metasurface. *Nature Communications*, 14(1):5377, 2023.
- [50] Yuanwei Liu, Xiao Liu, Xidong Mu, Tianwei Hou, Jiaqi Xu, Marco Di Renzo, and Naofal Al-Dhahir. Reconfigurable intelligent surfaces: Principles and opportunities. *IEEE communications surveys & tutorials*, 23(3):1546–1577, 2021.
- [51] Cheng Luo, Jie Hu, Luping Xiang, and Kun Yang. Reconfigurable intelligent sensing surface aided wireless powered communication networks: A sensing-then-reflecting approach. *IEEE Transactions on Communications*, 2023.
- [52] Weihan Li, Qian Ma, Che Liu, Yunfeng Zhang, Xianning Wu, Jiawei Wang, Shizhao Gao, Tianshuo Qiu, Tonghao Liu, Qiang Xiao, et al. Intelligent metasurface system for automatic tracking of moving targets and wireless communications based on computer vision. *Nature Communications*, 14(1):989, 2023.
- [53] Dexiao Xia, Lei Guan, Haixia Liu, Yajie Mu, Xin Wang, Jiaqi Han, Yan Shi, and Long Li. Metabreath: Multitarget respiration detection based on space-time-coding digital metasurface. *IEEE Transactions on Microwave Theory and Techniques*, 2023.
- [54] Xinyu Li, Jian Wei You, Ze Gu, Qian Ma, Jingyuan Zhang, Long Chen, and Tie Jun Cui. Multiperson detection and vital-sign sensing empowered by space-time-coding reconfigurable intelligent surfaces. *IEEE Internet of Things Journal*, 2024.
- [55] Zhiping Jiang, Tom H Luan, Xincheng Ren, Dongtao Lv, Han Hao, Jing Wang, Kun Zhao, Wei Xi, Yueshen Xu, and Rui Li. Eliminating the barriers: Demystifying wi-fi baseband design and introducing the picoscenes wi-fi sensing platform. *IEEE Internet of Things Journal*, 9(6):4476–4496, 2021.



**Qun Yan Zhou** received the B.E. degree in electronic science and technology from the Nanjing University of Aeronautics and Astronautics, Nanjing, China, in 2021. He is currently pursuing a Ph.D. degree with the State Key Laboratory of Millimeter Waves, Southeast University, Nanjing. His current research focuses on space-time-coding digital metasurface.



**Yimiao Sun** is currently pursuing a PhD. student at Tsinghua University. He received his B.E. degree from the University of Electronic Science and Technology of China (UESTC). His research interests include mobile computing and wireless sensing.



**Hui-Dong Li** (S'20-M'24) was born in Shijiazhuang, Hebei, China, in 1994. He received the B.S. and M.E. degrees in electrical engineering from Xidian University, Xi'an, China, in 2017 and 2020, respectively, and the Ph.D. degree in electrical and computer engineering from the University of Macau, Macau, SAR, China, in 2024. He has been a Post-Doctoral Fellow since April 2024 at The Hong Kong Polytechnic University, Hong Kong SAR, China. Currently, he is an Associate Professor with the State Key Laboratory of Millimeter Waves, Southeast University. His research interests include leaky-wave antennas, wireless power transfer, and metasurfaces. Dr Li received the best student paper awards of ACES 2023 and MTT-S IWS 2023 (finalist). He also serves as a Reviewer for several journals, including the IEEE Transactions on Antennas and Propagation and the IEEE Open Journal of Antennas and Propagation.



of Millimeter Waves, Southeast University, Nanjing 210096, China. His research interests mainly include intelligent signal processing and wireless communications.

**Jitong Ma** (Member, IEEE) received the B.S. degree in electronic information engineering from Hohai University, Nanjing, China, in 2013, and the M.S. degree in biomedical engineering from Dalian University of Technology, Dalian, China, in 2015, and the Ph.D. degree in signal and information processing from Dalian University of Technology, Dalian, China, in 2020. He is an associate professor with the Information Science and Technology College, Dalian Maritime University, Dalian, China. He is currently also a visiting scholar with the State Key Laboratory



**Yuan He** (Senior Member, IEEE) is an associate professor in the School of Software and BNRist of Tsinghua University. He received his B.E. degree from the University of Science and Technology of China, his M.E. degree in the Institute of Software, Chinese Academy of Sciences, and his PhD degree in Hong Kong University of Science and Technology. His research interests include wireless networks, Internet of Things, pervasive and mobile computing. He is a senior member of IEEE and a member of ACM.



**Yulong Chen** received his B.S. degree in the School of Software from Tsinghua University in 2022. He is currently pursuing a master's degree in software engineering at the same university. His research interests include mmWave sensing, Wi-Fi sensing, and RAN sensing.



**Si Ran Wang** received his Ph.D. degree in Electronic Information from the State Key Laboratory of Millimeter Waves, Southeast University, Nanjing, China, in 2024. He is currently a postdoctoral fellow at the State Key Laboratory of Terahertz and Millimeter Waves, City University of Hong Kong. His research interests focus on information metamaterials and metasurfaces.



**Qiang Cheng** (Senior Member, IEEE) received the B.S. and M.S. degrees from the Nanjing University of Aeronautics and Astronautics, Nanjing, Jiangsu, China, in 2001 and 2004, respectively, and the Ph.D. degree from Southeast University, Nanjing, in 2008. In 2008, he joined the State Key Laboratory of Millimeter Waves, Southeast University. He is the chief professor of Southeast University, deputy director of the State Key Laboratory of Millimeter Wave, winner of the National Natural Science Foundation Outstanding Youth Fund, Young Scholar of Changjiang Scholars Award Program, and the first batch of Outstanding Youth Fund in Jiangsu Province. He is supported by the New Century Outstanding Talents Support Program of the Ministry of Education, Jiangsu Province 333 Talent Project, and Jiangsu Province Six Talent Peak Program. Senior member of IEEE, and engaged in electromagnetic metamaterial research for a long time, selected as a citation scholar of Creonly Safety. His research work was selected as the second prize of the National Natural Science Award in 2014 and 2018, the First Prize of the Natural Science Award of the Ministry of Education in 2011, and the Top Ten Scientific and Technological Progress of Chinese Universities in 2021.



**Jun Yan Dai** received the B.S. degree in information engineering from Southeast University, Nanjing, China, in 2013, and the Ph.D. degree in electromagnetic field and microwave technology from the State Key Laboratory of Millimeter Waves, Southeast University, in 2019. From February 2020 to December 2021, he was a Post-Doctoral Fellow with the State Key Laboratory of Terahertz and Millimeter Waves, City University of Hong Kong, Hong Kong. He is currently an Associate Professor with the State Key Laboratory of Millimeter Waves, Southeast University. His research interests include metasurfaces, reconfigurable intelligent surfaces, space-time modulation technology, and wireless communication systems.